

Monotone level-sets on arbitrary meshes without redistancing

Ido Akkerman

*Mechanical, Maritime and Materials Engineering Department
Delft University of Technology*

Abstract

In this paper we present approaches that address two issues that can occur when the level-set method is used to simulate two-fluid flows in engineering practice.

The first issue concerns regularizing the Heaviside function on arbitrary meshes. We show that the regularized Heaviside function can be non-smooth on non-uniform meshes. Alternative regularizing definitions that are indeed smooth and monotonic, are introduced. These new definitions lead to smooth Heaviside functions by taking the changing local meshsize into account.

The second issue is the computational cost and fragility caused by the necessity of redistancing the level-set field. In [1, 2] it is shown that strongly coupling the level-set convection with the flow solver provides robustness and potentially efficiency and accuracy advantages. The next step would be to include redistancing within the strong coupling part of the algorithm. The computational cost of current redistancing procedure prohibit this. Four alternative approaches for circumventing the expensive redistancing step are proposed. This should facilitate a fully coupled level-set approach.

Some benchmark cases demonstrate the efficacy of the proposed approaches. These includes the standard test case of the vortex in a box. Based on these results the most favourable redistancing approach is selected.

Keywords: level-set, arbitrary meshes, smooth Heaviside, implicit redistancing

1. Introduction

Level-sets are a very powerful approach for solving interface problems [3]. By disconnecting the interface description from the underlying mesh, topology changes of the interface are handled with ease. For numerical reasons, such as numerical quadrature or finite differencing, the interface is often given a finite mesh-dependent width. This is done by adopting a so-called regularized Heaviside function, where the transition from zero to unity does not occur instantaneously but over a finite band. This regularization, however, causes two problems. On irregular meshes – which might occur in the analysis of engineering artefacts – the smoothed Heaviside can become non-smooth or even non-monotone. Additionally, the level-set is required to be a distance function in order to control the thickness of the interface. Due to its evolution the level-set evolves requires to be redistanced, that is the distance property needs to be actively repaired.

In [1, 2] the level-set method is used to model a rigid-body floating on a water surface. This water surface is handled using a level-set. In this paper we adopted a strongly coupled modeling approach. Meaning that both the flow; interface evolution; body motion and mesh deformation are solved simultaneously. In agreement with [4, 5, 6] – and other FSI literature – this approach results in a robust solution strategy. In a pure two-fluid problem, i.e. without a floating object, the strongly coupled approach proved to be more robust than traditional approaches where interface evolution is solved after the flow problem is solved.

However, the redistancing of the level-set was not included in the strongly coupled part of the solver, this was done at the end of each time step. Due to the redistribution of mass associated with redistancing, momentum and energy conservation are difficult to control. Certainly, the energy errors are troublesome as these might trigger instabilities in the solver. Therefore, there is a desire to include the redistancing step in the strongly coupled part of the method. This should allow methods that are either energy conservative or guaranteed to be energy dissipative. This is envisioned to lead to more robust and more accurate methods.

In this paper we present four alternative approaches which lead to an approximate distance field without directly solving a redistancing problem. These approaches are formulated in such a way that they potentially solve the non-smoothness on irregular grids.

The paper is structured as follows, in section 2 provides a short introduction to the level-set method and the regularized Heaviside function. In section 3 we show that a naive definition of the regularized Heaviside can actually be non-smooth. A potential solution to this problem is presented.

In section 4 we build on the result from the previous section and introduce four alternative approaches to redistance the level-set field. All these approaches circumvent solving the difficult non-linear Eikonal equation. The Eikonal equation is translated to simple projection problems that achieve the same: a distance field suitable to define a smooth Heaviside.

In section 5 we give a short description of the numerical formulations and the finite element and isogeometric discretizations employed to solve the convection and redistancing problems in the next section. In this section, section 6, we first solve a simple redistancing problem on irregular grids and then solve the vortex in a box problem using different discretizations and different redistancing approaches. Using these test cases we identify the best method, and the appropriate numerical parameters. For this method a mesh convergence study is performed and suitability in three dimensions is tested.

In section 7 we conclude and sketch a perspective for further use of the proposed methods

2. The level set method

The level-set method has since its origin [3] been applied to numerous problems involving surfaces, interfaces and shapes. Its application can be found in a wide range of areas from image processing, computer graphics, topology and shape optimisation and simulation of physics problems at interfaces such as crystal growth, or two-fluid flow.

See, the review papers [7, 8] or books [9, 10] for a broad picture of the applications and methods available. In this paper we focus on level-set in combination with variational methods such as finite element and isogeometric analysis [11] with the final goal of applying it to two-fluid flow. The two-fluid problem is a physical problem where the interface between the fluids is unknown and physical parameters are discontinuous across the interface. Adoption of a level-set allows for easy handling of interface topology changes and regularisation of the discontinuity.

2.1. Level-sets for two-fluid problems

In the level-set method a surface of lower dimension, such as an interface between two distinct materials is indirectly parameterized employing a globally defined function. This function is denoted as ϕ , and defines a surface as follows,

$$\Gamma_i = \{\mathbf{x} \in \Omega : \phi = 0\}. \quad (1)$$

This automatically leads to the following distinct subdomains,

$$\begin{aligned} \Omega^- &= \{\mathbf{x} \in \Omega : \phi < 0\}, \\ \Omega^+ &= \{\mathbf{x} \in \Omega : \phi > 0\}, \end{aligned} \quad (2)$$

which allows the prescription of different physical parameters in each subdomain. For instance, the density

$$\rho = \begin{cases} \rho_0 & \text{if } \mathbf{x} \in \Omega^-, \\ \rho_1 & \text{if } \mathbf{x} \in \Omega^+. \end{cases} \quad (3)$$

Alternatively, the Heaviside function

$$H(\phi) = \begin{cases} 0 & \text{if } \phi < 0, \\ \frac{1}{2} & \text{if } \phi = 0, \\ 1 & \text{if } \phi > 0, \end{cases} \quad (4)$$

can be used for a convex interpolation to define a density

$$\rho = \rho_0(1 - H(\phi)) + \rho_1 H(\phi). \quad (5)$$

This has the advantage of automatically handling the interface itself in a natural way.

2.2. Regularized Heaviside

In numerical methods the sharp interfaces defined in the previous section can lead to problems. For instance this appears when determining a mass matrix, M_{ab} is approximated by quadrature as,

$$M_{ab} = \int_{\Omega} \rho N_a N_b d\Omega \approx \sum_{i=1..n_{ip}} \rho(\mathbf{x}_i) N_a(\mathbf{x}_i) N_b(\mathbf{x}_i) w_i. \quad (6)$$

A sudden change of the density leads to a very bad approximation of the intended integral.

To alleviate this problem the sharp Heaviside function, defined in eq (4), is replaced by a regularized Heaviside function. This regularized Heaviside function is often defined as

$$H_{\epsilon}(\phi) = \begin{cases} 0 & \text{if } \phi < -\epsilon, \\ \frac{1}{2}(1 + \sin(\frac{\pi\phi}{2\epsilon})) & \text{if } \phi = 0, \\ 1 & \text{if } \phi > \epsilon, \end{cases} \quad (7)$$

where ϵ is the smoothing distance. Instead of an instantaneous switch from 0 to 1, this switch is spread over a finite layer around the interface. To have strict control over the width of this interface layer, we require ϕ , to be a signed distance function. This means it needs to satisfy

$$\|\nabla\phi\| = 1, \quad (8)$$

which is the Eikonal equation. As the regularizing is introduced to deal with numerical issues, such as quadrature, it is natural to specify the finite interface layer in terms of mesh size h as

$$\epsilon = \alpha h. \quad (9)$$

Here α is an $O(1)$ parameter. The meshsize can be defined unambiguously for structured equidistant meshes. However, on arbitrary meshes this is not always straightforward. In [12, 13, 1] we employed the meshsize

$$h = \frac{\|\nabla\phi\|}{\sqrt{\nabla\phi \cdot \mathbf{G}\nabla\phi}}, \quad (10)$$

where \mathbf{G} is the metric-tensor

$$\mathbf{G} = \left(\frac{\partial\xi}{\partial\mathbf{x}} \right)^T \frac{\partial\xi}{\partial\mathbf{x}} \quad (11)$$

where \mathbf{x} is the physical space coordinate and ξ is the coordinate in parametric space pertaining to the reference element.

This definition of h incorporates the desired directional information. Effectively, a length scale is extracted from the metric-tensor in the direction $\frac{\nabla\phi}{\|\nabla\phi\|}$.

3. Monotonicity on arbitrary meshes

In this section we further discuss the smoothing of the Heaviside function on arbitrary meshes. For this exposition it is useful to slightly rewrite the regularized Heaviside function,

$$\hat{H}(\hat{\phi}) = \begin{cases} 0 & \text{if } \hat{\phi} < -\alpha, \\ \frac{1}{2}(1 + \sin(\frac{\pi}{2} \frac{\hat{\phi}}{\alpha})) & \text{if } \hat{\phi} = 0, \\ 1 & \text{if } \hat{\phi} > \alpha, \end{cases} \quad (12)$$

where

$$\hat{\phi} = \frac{\phi}{h} \tag{13}$$

is the scaled distance. In other words, if ϕ is the *actual* distance to the interface, expressed in for instance *mm* or *m*, then $\hat{\phi}$ can be thought of as that same distance but expressed in *number of elements*, that is a multiple of a typical element length. However, since this scaling occurs locally, the variation of h along the path - from interface to the point under consideration - is not taken into account. Therefore, this rescaled distance is only an effective estimate if h varies only mildly (or not at all) across the interface.

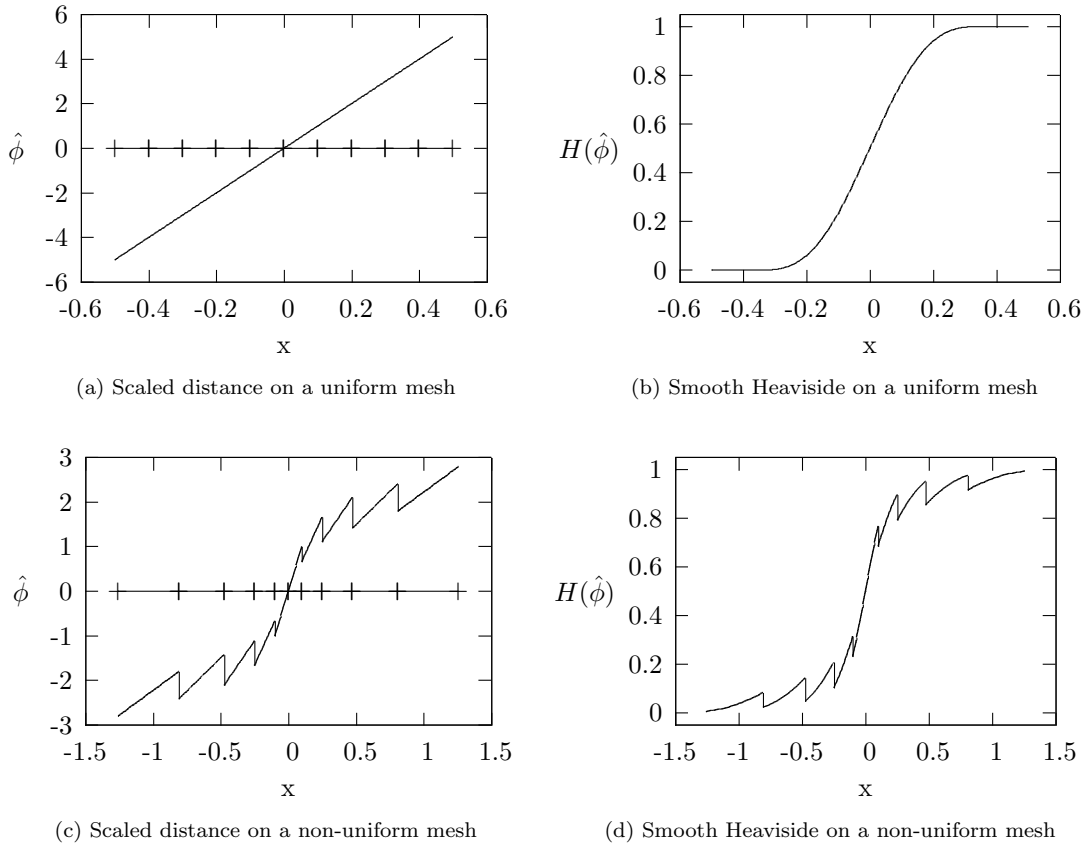


Figure 1: Original scaled distance and regularized Heaviside on a uniform and non-uniform mesh.

Figure 1 visualizes the scaled distance and the resulting regularized Heaviside function on an uniform and non-uniform mesh, respectively. The element distribution is indicated in the two left figures. The top plots show the results on a uniform mesh. In this case the scaled distance is a straight line and the regularized Heaviside function is indeed smooth. The bottom plots show the results obtained on a non-uniform mesh. Here the scaled distance and more importantly the regularized Heaviside function show a saw-tooth behaviour. This defeats the purpose of the regularization. Although, one could argue that the quadrature on each element behaves well as the jumps occur at element interfaces. This is indeed the case, however, this will result in an inconsistent numerical method unless the density jumps at the interface are handled correctly, i.e. analogous to in the discontinuous Galerkin method [14].

3.1. Path dependent rescaling

In order to solve the problems indicated in the previous section. We should translate eq (13) to a pure local relation as

$$d\hat{\phi} = \frac{d\phi}{h}. \quad (14)$$

The total scaled distance can be found by path integration,

$$\hat{\phi} = \int \frac{d\phi}{h} \quad (15)$$

which is not trivial to compute in practice.

Instead we take another route to obtain $\hat{\phi}$. As an alternative to eq (14) we can also state,

$$\nabla\hat{\phi} = \frac{\nabla\phi}{h}. \quad (16)$$

This immediately results in an alternative Eikonal equation for the scaled distance:

$$\|\nabla\hat{\phi}\| = \frac{\|\nabla\phi\|}{h} = \frac{1}{h}, \quad (17)$$

where we used $\|\nabla\phi\| = 1$. In principle any reasonable selection of h will work.

However, inspired on the definition for h given in eq (10), we can define h in such a way that eq (17) gets replaced with an attractive alternative Eikonal equation. To achieve this we choose

$$h = \frac{\sqrt{\nabla\hat{\phi} \cdot \mathbf{G}^{-1} \nabla\hat{\phi}}}{\|\nabla\hat{\phi}\|}, \quad (18)$$

where

$$\mathbf{G}^{-1} = \frac{\partial \mathbf{x}}{\partial \xi} \left(\frac{\partial \mathbf{x}}{\partial \xi} \right)^T \quad (19)$$

is the inverse of the metric-tensor defined in eq (11). The same rationale behind eq (10) is employed eq (18). We use the direction $\frac{\nabla\hat{\phi}}{\|\nabla\hat{\phi}\|}$ to extract the relevant mesh size from the inverse metric tensor. The metric tensor depends on the rotation, scaling and distortion of the element and are naturally included in the mesh size definition.

Defining ∇_{ξ} as the gradient in the reference direction, we can use the chain rule to arrive at

$$\nabla_{\xi}\hat{\phi} \equiv \frac{\partial\hat{\phi}}{\partial\xi} = \frac{\partial\hat{\phi}}{\partial\mathbf{x}} \frac{\partial\mathbf{x}}{\partial\xi} = \nabla\hat{\phi} \frac{\partial\mathbf{x}}{\partial\xi}, \quad (20)$$

This is substituted into eq (18) to obtain

$$h = \frac{\|\nabla_{\xi}\hat{\phi}\|}{\|\nabla\hat{\phi}\|}. \quad (21)$$

Combining this with the scaled Eikonal equation (17) we get

$$\|\nabla_{\xi}\hat{\phi}\| = 1, \quad (22)$$

which is the Eikonal equation in terms of the parametric space. This equation states that $\hat{\phi}$ is a distance in terms of mesh lengths, which was exactly what we were looking for in the first place.

Figure 2 shows the resulting scaled distance and regularized Heaviside when the alternative scaling is used. The mesh is the same as in figure 1. Both the distance and Heaviside function do not show a saw-tooth behaviour and the Heaviside function is actually smooth, as intended. The scaled distance is indeed not a straight line, which is caused by the metric defined by the non-uniform mesh.

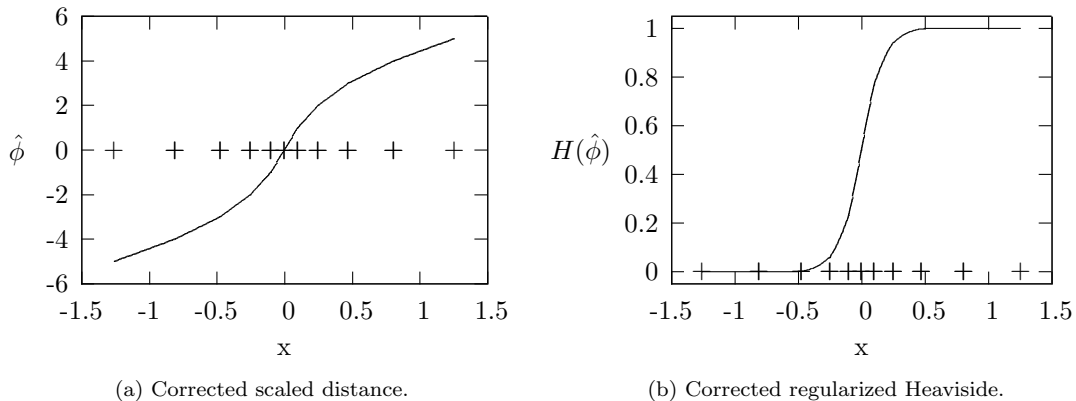


Figure 2: Modified scaled distance and regularized Heaviside on non-uniform mesh.

4. Circumventing explicit redistancing

In the previous section we have addressed the issue of monotone smoothing of the Heaviside function. An equally important issue is that of the distance property of ϕ , or better of $\hat{\phi}$. The level-set time-evolution is typically given by

$$\frac{\partial \phi}{\partial t} + \mathbf{u} \cdot \nabla \phi = 0 \quad (23)$$

or something equivalent. It is not guaranteed whether its distance property is maintained during the simulation. In order to keep explicit control of the interface layer thickness, we need to restore the distance property. Even if ϕ would remain a distance function, the path dependent scaling of the distance function still requires us to solve an Eikonal equation, namely eq (22),

$$\|\nabla_{\xi} \hat{\phi}\| = 1 \quad \text{on } \Omega^- \cup \Omega^+. \quad (24)$$

This equation is augmented with the following embedded boundary condition,

$$\hat{\phi} = 0 \quad \text{on } \Gamma_i = \{\mathbf{x} \in \Omega : \phi = 0\}, \quad (25)$$

which forces the interface to remain fixed in the scaling/redistancing step.

Many different approaches to solve the Eikonal equation have been developed, see for instance [15] and references therein. Most methods introduce a pseudotime τ and march in time using

$$\frac{\partial \hat{\phi}}{\partial \tau} + \mathbf{a} \cdot \nabla \hat{\phi} = S, \quad (26)$$

where \mathbf{a} is an effective convection velocity and S is a source. Both \mathbf{a} and S are carefully chosen to guarantee convergence towards the desired solution.

Remark: to guarantee a steady state solution the source term needs to include a term penalizing the deviation of the interface, as shown in [1]. This issue is often circumvented by limiting the number of pseudotime steps.

This redistancing procedure has several drawbacks. It is quite costly, even when limited in space (only redistance near the interface) or time (only redistance every so many timesteps). Additionally, careful attention needs to be paid to the interplay of different parameters associated with the time-marching algorithm. This makes the procedure somewhat fragile. Last but not least, it is difficult to find the right balance between redistancing on the one hand and maintaining the interface on the other hand. Therefore, it is preferred to circumvent explicit redistancing.

4.1. General idea

In the following sections we present four alternative procedures to achieve this. All four alternatives hinge on the idea that we relate the unknown $\hat{\phi}$ with the known ϕ by

$$\hat{\phi} = \phi\epsilon, \quad (27)$$

where ϵ is an unknown multiplicative scaling, which is required to be strictly positive. Clearly, $\hat{\phi}$ vanishes when ϕ vanishes. This means that the interface location is trivially conserved. There is no need to balance redistancing with maintaining the interface.

The multiplicative scaling can be found by enforcing the Eikonal equation in parametric space (22),

$$\|\nabla_{\xi}\hat{\phi}\| = 1 \quad \text{on} \quad \Omega^{-} \cup \Omega^{+} \quad (28)$$

and subsequently applying the chain rule. As we are only interested in what happens near the interface we assume $\phi \approx 0$ which results in the following relation for the multiplicative scaling,

$$\epsilon = \frac{1}{\|\nabla_{\xi}\phi\|} \quad (29)$$

In the following section four different alternative approaches based on this general idea are presented.

4.2. First alternative: Direct redistancing

The first option is straightforward pointwise scaling:

$$\hat{\phi} = \frac{\phi}{\|\nabla_{\xi}\phi\|} \quad (30)$$

This has the risk of resulting in divisions by zero. Additionally, on standard C_0 continuous discretizations this will likely lead to a discontinuous $\hat{\phi}$ field and consequently a discontinuous $H(\hat{\phi})$ field. Therefore this does not seem to be an attractive option.

4.3. Second alternative: Projected redistancing

We can obtain a continuous distance field by projecting the discontinuous $\hat{\phi}$ of the previous section on a C_0 discretization. This can be done by solving the following projection problem

$$\hat{\phi} - \nabla_{\xi}\kappa_d\nabla_{\xi}\hat{\phi} = \frac{\phi}{\|\nabla_{\xi}\phi\|}, \quad (31)$$

or by solving the following equivalent weak form:

Find $\hat{\phi} \in \mathcal{V}^h$ such that:

$$(w, \hat{\phi})_{\Omega} + (\nabla_{\xi}w, \kappa_d\nabla_{\xi}\hat{\phi}) = \left(w, \frac{\phi}{\|\nabla_{\xi}\phi\|} \right)_{\Omega} \quad \forall w \in \mathcal{V}^h. \quad (32)$$

Here, and in the remainder of this paper, κ_d is a smoothing parameter and \mathcal{V}^h is an appropriate discrete space. Due to the projection and the associated discretization errors, the interface location remains at the same position in an approximate sense. This means the interface is not necessarily maintained during the redistancing step.

4.4. Third alternative: Projected scaling

By projecting the scaling coefficient on a continuous discretization the properties of continuity and interface conservation can be achieved simultaneously. This can be achieved by either the following projection,

$$\epsilon - \nabla_{\xi} \kappa_d \nabla_{\xi} \epsilon = \frac{1}{\|\nabla_{\xi} \phi\|} \quad (33)$$

or by solving the equivalent weak form:

Find $\epsilon \in \mathcal{V}^h$ such that:

$$(w, \epsilon)_{\Omega} + (\nabla_{\xi} w, \kappa_d \nabla_{\xi} \epsilon) = \left(w, \frac{1}{\|\nabla_{\xi} \phi\|} \right)_{\Omega} \quad \forall w \in \mathcal{V}^h. \quad (34)$$

The sought after distance field can easily be computed as,

$$\hat{\phi} = \phi \epsilon. \quad (35)$$

4.5. Fourth alternative: Projected inverse scaling

The last alternative approach is a small modification of the previous alternative. Instead of projecting the multiplicative correction, we project its reciprocal value. This is achieved with the projection,

$$\epsilon - \nabla_{\xi} \kappa_d \nabla_{\xi} \epsilon = \|\nabla_{\xi} \phi\| \quad (36)$$

or by solving its corresponding weak form,

Find $\epsilon \in \mathcal{V}^h$ such that:

$$(w, \epsilon)_{\Omega} + (\nabla_{\xi} w, \kappa_d \nabla_{\xi} \epsilon) = (w, \|\nabla_{\xi} \phi\|)_{\Omega} \quad \forall w \in \mathcal{V}^h \quad (37)$$

The sought after distance field is computed as

$$\hat{\phi} = \frac{\phi}{\epsilon}, \quad (38)$$

in this case.

5. Numerical algorithm

In order to solve the convection problem given in eq (23) we choose to use finite elements and isogeometric analysis. For completeness we describe the adopted weak formulation and associated numerical parameters. Next, we briefly discuss the isogeometric analysis shape functions that are used. Adoption of isogeometric analysis allows the selection of C_1 continuous discretizations. This will turn out to be beneficial.

5.1. SUPG formulation

The convective problem from eq (23) is solved using a SUPG formulation [16]. This problem is stated as follows:

Find $\phi \in \mathcal{V}^h$ such that:

$$(w + \tau \mathbf{u} \cdot \nabla w, \phi_t + \mathbf{u} \cdot \nabla \phi)_{\Omega} + (\nabla_{\xi} w, \kappa_c \nabla_{\xi} \phi)_{\Omega} = 0 \quad \forall w \in \mathcal{V}^h \quad (39)$$

where \mathcal{V}^h is an appropriate discrete space, τ is the stabilisation parameter computed as

$$\tau = (\Delta t^2 + \mathbf{u} \cdot \mathbf{G}\mathbf{u})^{-1/2}, \quad (40)$$

and κ_c is the discontinuity capturing parameter computed as

$$\kappa_c = C |\phi_t + \mathbf{u} \cdot \nabla \phi|, \quad (41)$$

where C is an $O(1)$ parameter. Note that the residual-based nature choice of the discontinuity capturing parameter leads to a strongly consistent method. This discontinuity capturing is inspired on similar discontinuity capturing reported in [17] and is dimensionally consistent with more traditional discontinuity capturing parameter such as reported in for instance [18, 19].

The equations are integrated in time with the Crank-Nicolson method. The resulting nonlinear system is solved with PETSc [20, 21].

5.2. Volume conservation

Often, for instance when dealing with incompressible fluids, it is known *a priori* that the volume of each subdomain, given by

$$\begin{aligned} V_0 &= \int_{\Omega} 1 - H(\hat{\phi}) d\Omega, \\ V_1 &= \int_{\Omega} H(\hat{\phi}) d\Omega, \end{aligned} \quad (42)$$

is conserved. This mass conservation is not guaranteed in the discrete setting. Due to accumulation of volume errors one constituent can completely disappear in extreme situations. To avoid this we add a global constant to our convected level-set field ϕ which restores global conservation. This global constant follows from solving the following non-linear equation:

$$\int_{\Omega} H(\hat{\phi}(\phi^{n+1} + \phi'^{n+1})) d\Omega = \int_{\Omega} H(\hat{\phi}(\phi^n + \phi'^n)) d\Omega \quad (43)$$

A simple Newton-Raphson procedure is employed to find this solution. This routine is quite fast as this is a scalar equation.

For convenience we introduce the mass correction in the time derivative of the overall convection problem. The approximation for time derivative is given by

$$\phi_t = \frac{\phi^{n+1} - (\phi^n + \phi'^n)}{\Delta t}. \quad (44)$$

In this way ϕ'^{n+1} as an instantaneous correction necessary for maintaining mass conservation.

5.3. Isogeometric analysis

Isogeometric analysis, introduced in [11], is the idea to directly employ shape functions from CAD in simulations. Since its introduction a large body of research is directed towards this general concept, see for instance [22] and references there in. One of the more popular choices for CAD shape functions are the so-called NURBS [23]. In this work NURBS will be employed as well.

Approximation properties similar to those of standard finite elements can be proved [24]. Furthermore, NURBS show superior convergence properties in terms of accuracy per degree of freedom [25]. A large body of work exist confirming the benefits of adopting NURBS shapefunctions – or isogeometric analysis in general.

6. Numerical experiments

6.1. Distortion test

To assess the four alternative approaches for redistancing we apply these to distorted meshes. The meshsize is uniformly reduced toward both the x and y axes. The underlying level-set functions, given by,

$$\phi = x - y \quad (45)$$

result in an interface from the bottom left to the top right.

The contour lines of the Heaviside due to the redistancing in terms of the mesh length is given in figures 3, 4, 5 and 6. To exaggerate the results we have selected a relatively wide interface width, namely $\alpha = 3$.

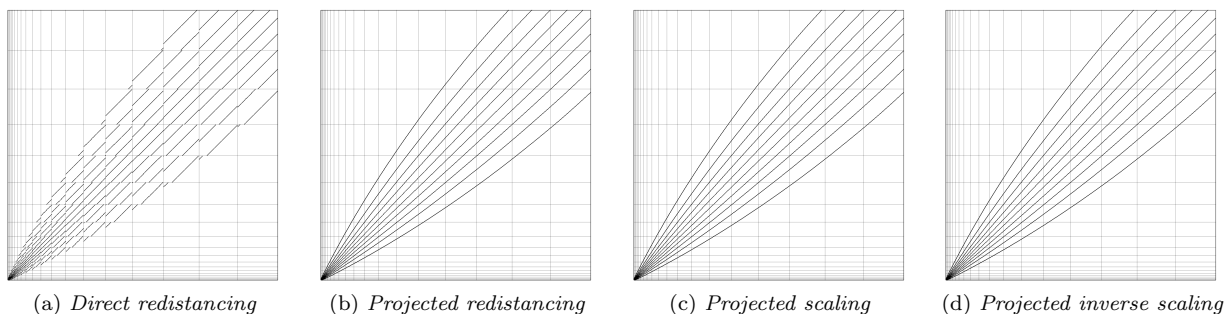


Figure 3: Contour lines for the different redistancing approaches, all results are on a $C_1 - Q_2$ mesh without any smoothing.

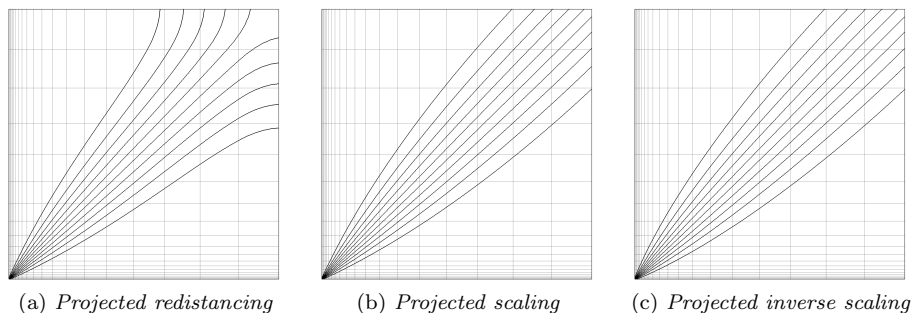


Figure 4: Contour lines for the different projection approaches, all results are on a $C_1 - Q_2$ mesh with smoothing $\kappa_d = 1$.

In figure 3 the contours for all four methods on a $C_1 - Q_2$ mesh are presented. From this it can be clearly seen that the *direct redistancing* results in a discontinuous Heaviside, illustrated by the contour lines that terminate at element edges. This shows that even on C_1 meshes the direct scaling does not necessarily provide a smooth Heaviside. For the other three approaches the contour lines are nicely continuous and there is hardly any distinction between the three projection based methods. On a $C_0 - Q_1$ mesh the result for all four approaches will look analogous.

In figure 4 the effect of moderate smoothing is presented. *Projected redistancing* clearly suffers from this inclusion of smoothing, while the two scaled projection methods are largely unaffected. Although for *projected inverse scaling* the contour lines converge less at the origin due to the smoothing. With increased smoothing *projected inverse scaling* suffers more from this effect, as shown in figure 5.

In figure 6 the two scaled projection methods on a triangular mesh are presented. The triangular meshes are generated with gmsht [26] In this case the irregularity of the triangular meshes highly favours the inclusion of some modest smoothing.

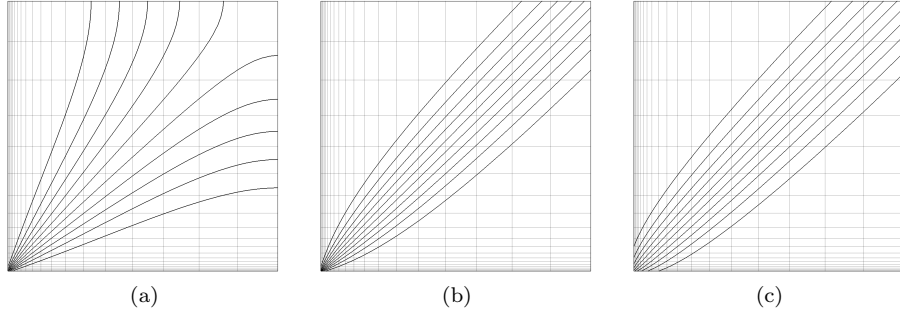


Figure 5: Contour lines for the scaling approaches, all results are on a $C_1 - Q_2$ mesh with high smoothing $\kappa_d = 10$.

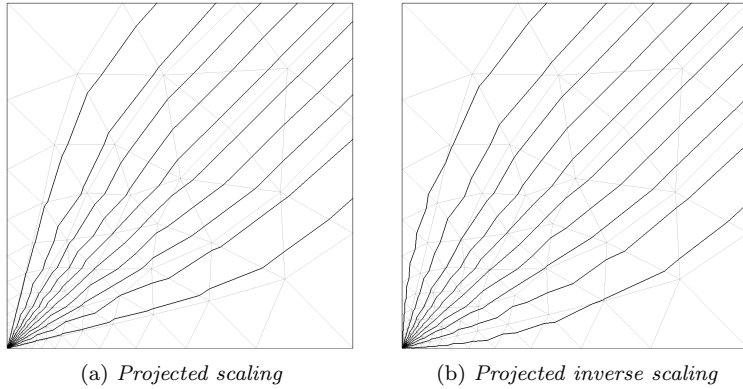


Figure 6: Contour lines for the different redistancing approaches on a triangular mesh with smoothing $\kappa_d = 1$.

6.2. Problem description: Vortex in a box

To assess the efficacy of the proposed redistancing approaches we apply all methods on the vortex in a box problem. We focus only on the three projection-based alternatives, as the direct approach fails to deliver smooth Heaviside functions.

The problem setup originates from [27] while the parameters are taken from [28]. The computational domain is a unit square and ϕ is initialized such that its zero level set is a circular disc of radius 0.15 centered at $(0.50, 0.75)$. The time-dependent velocity $\mathbf{u} = (u, v)$, is given by

$$\begin{aligned} u &= \cos\left(\frac{\pi t}{8}\right) \sin(2\pi y) \sin(\pi x)^2, \\ v &= -\cos\left(\frac{\pi t}{8}\right) \sin(2\pi x) \sin(\pi y)^2. \end{aligned} \tag{46}$$

This velocity field stretches the disc into a very thin spiral until $t = 4$, next the flow reverses and the spiral is deformed back into a perfect circle at $t = 8$.

We solve this problem on different meshes. On the one hand we have a sequence of quadrilateral NURBS elements with linear- C_0 or quadratic- C_1 tensor product based shape functions. Additionally, we solve the problem on triangular elements, which indicates the generality of the approach.

We select an 80×80 element NURBS meshes and an equivalent triangular mesh with 16794 linear elements and 8558 nodes. For the triangular mesh the target line element count along an domain edge is identical to the that of the NURBS meshes. This mesh size is selected because it is sufficiently accurate to

draw meaningful conclusions, while on the other hand it is still coarse enough to see the numerical errors and judge the behaviour of the methods with the naked eye.

6.3. Projected redistancing

Figure 7 shows snapshots of the regularized Heaviside at maximum distortion for the different smoothing parameters κ for a 80×80 C_0 linear mesh.

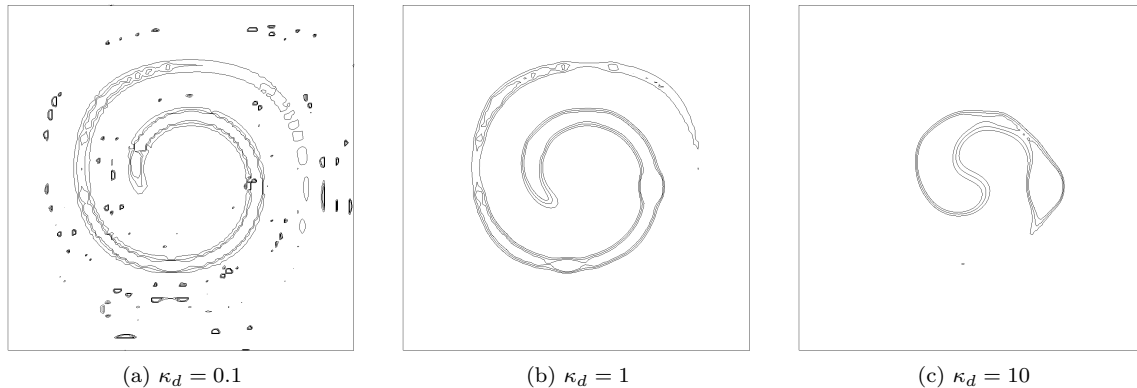


Figure 7: Contour plots of the regularized Heaviside for *projected redistancing* on a 80×80 C_0 linear mesh.

It can be seen there is a delicate balance between not enough and too much smoothing. When κ_d is small there is not enough smoothing and the distance field shows oscillations, while for the higher values of κ_d the diffusion caused by the smoothing moves the interface more than desired. For the other discretizations – P_1 triangles and $C_1 - Q_2$ quadrilaterals – we get similar results, leading to the same conclusion.

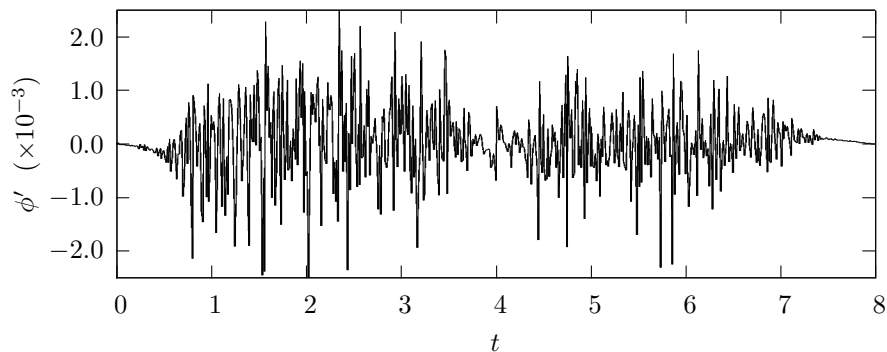


Figure 8: Correction required for volume conservation for the 80×80 linear mesh with $\kappa_d = 1$.

For all simulations the volume is conserved up to machine precision, even when the solution is highly deformed due to the smoothing. This demonstrates effectiveness of the volume correction method presented in section 5.2. The correction required for volume conservation is of the order 10^{-3} per time step. A typical time trace of this correction is given in figure 8.

6.4. Projected scaling

Figure 9 shows snapshots of the regularized Heaviside at maximum distortion for the different smoothing parameters κ_d for a 80×80 C_0 linear mesh.

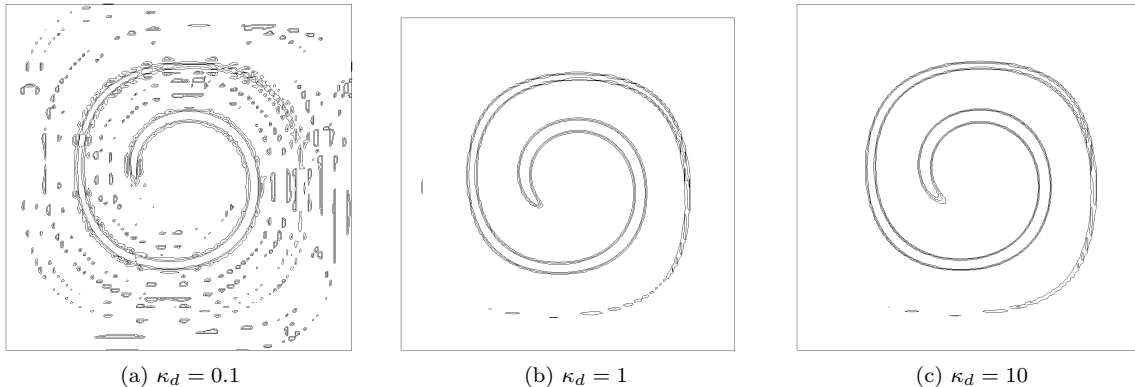


Figure 9: Contour plots of the regularized Heaviside for *projected scaling* on a 80×80 C_0 linear mesh.

It can be seen that for this approach there is no problem when a large smoothing parameter is used. However, when the smoothing parameter is too small the solution becomes spotty and irregular similar as in the previous section. This monotone behaviour with respect to the smoothing parameter makes this a viable approach. For the other discretizations – P_1 triangles and $C_1 - Q_2$ quadrilaterals – we get similar results, leading to the same conclusion.

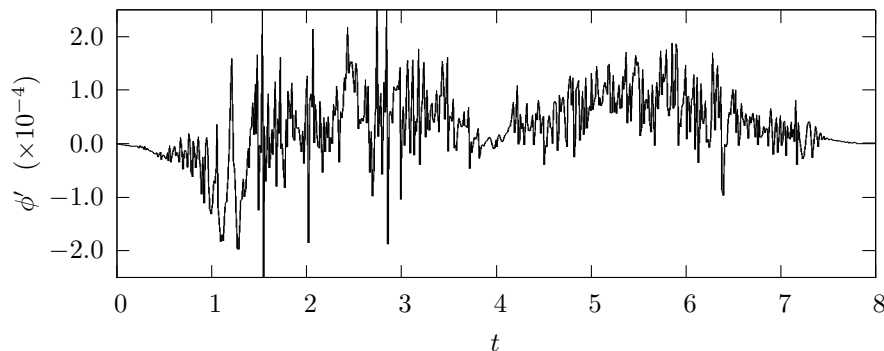


Figure 10: Correction required for volume conservation for the 80×80 linear mesh with $\kappa_d = 1$.

The interface conservative nature of the redistancing approach is also apparent in the time trace of the correction parameter required to conserve volume. A typical time trace is depicted in figure 10. Comparing with the time trace of the previous section, in figure 8, the required correction is roughly an order of magnitude less.

6.5. Projected inverse scaling

Figure 11 shows snapshots of the regularized Heaviside at maximum distortion for the different smoothing parameters κ for a $80 C_0$ linear mesh. The smoothing does not have a significant influence on the results. Both high and low smoothing limits display acceptable answers.

Figure 12 shows the contours for the same smoothing range but now on the $C_1 - Q_2$ mesh. The results are very similar. For the triangular mesh the results, as shown in figure 13, are less smooth due to unstructured nature of the mesh. Therefore, regularization has a more pronounced effect for this mesh. The higher κ_d results in better and smoother answers. However, as shown in section 6.1 there is also an upper limit to the desired smoothing.

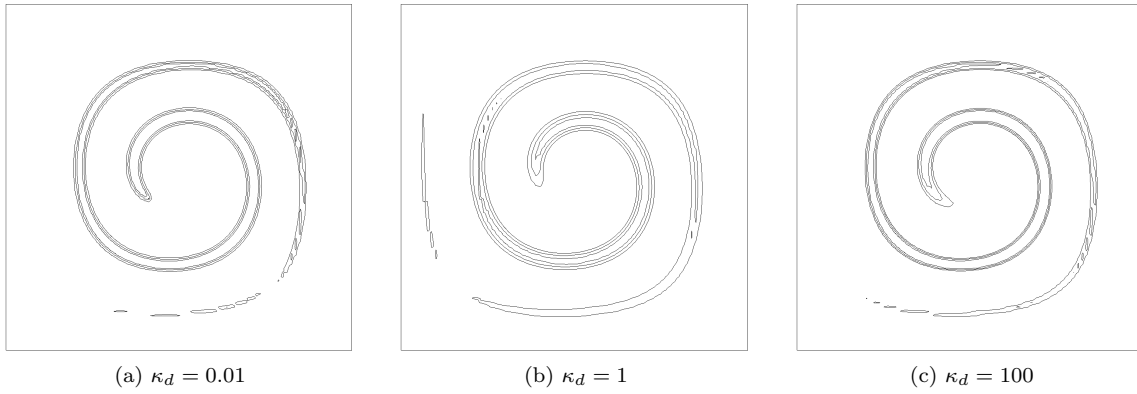


Figure 11: Contour plots of the regularized Heaviside for *projected inverse scaling* on a 80×80 C_0 linear mesh.

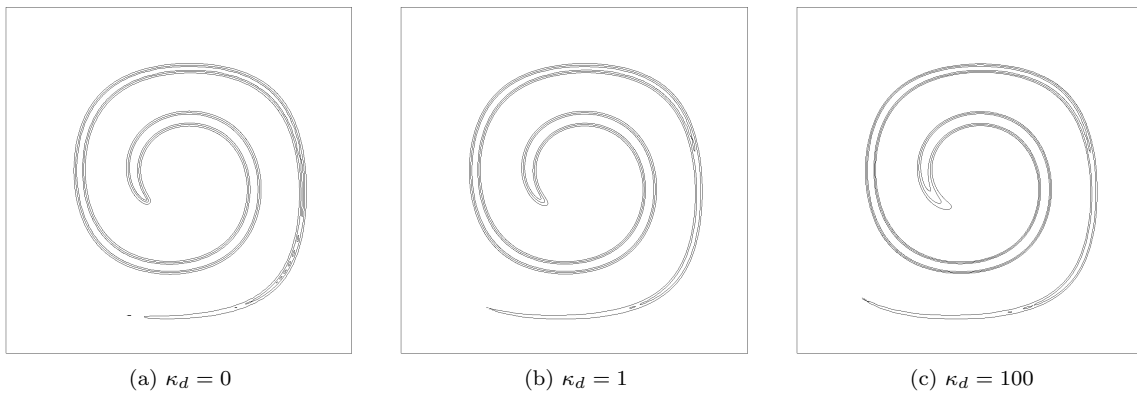


Figure 12: Contour plots of the regularized Heaviside for *projected inverse scaling* on a 80×80 C_1 quadratic mesh.

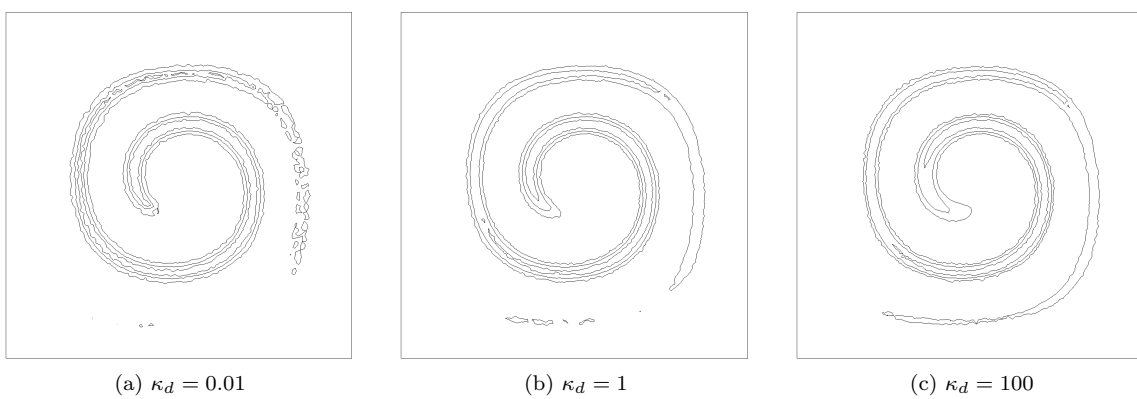


Figure 13: Contour plots of the regularized Heaviside for *projected inverse scaling* on a triangular mesh with 4541 elements.

The better behaviour of the *projected inverse scaling* compared with the *projected scaling* is also apparent

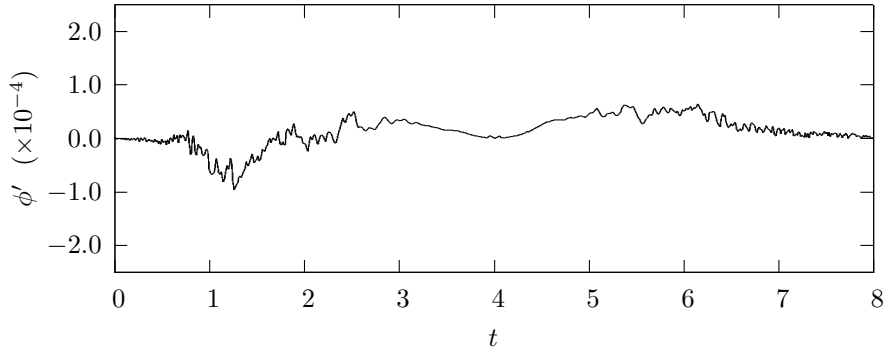


Figure 14: Correction required for volume conservation for the 80×80 linear mesh with $\kappa_d = 1$.

when considering the time trace of the correction required for volume conservation, see figure 14. This correction is smaller, but also varies significantly less violent.

6.6. Convergence study

Using the results from the previous sections we focus our attention on the approaches that showed the most potential. This is *projected inverse scaling* which is suitable for all mesh types. For the quadrilateral meshes, the smoothing is absent, that is $\kappa_d = 0$, while for the triangular mesh we use a relatively high smoothing of $\kappa_d = 10$. The previous paragraph indicates these smoothing values lead to satisfying results.

In this section we investigate the convergence of this approach. We consider two different measures for the accuracy of the solution at the final time $t = 8$. First, we look at the area mismatch between actual and anticipated area indicated by the level-set. The anticipated value is the initial area, i.e. at $t = 0$. This measure is computed as

$$L_1(\hat{H}) = \int_{\Omega} |H(\hat{\phi}_T) - H(\hat{\phi}_0)| d\Omega, \quad (47)$$

and is physically the most relevant in future applications.

Additionally, we look how far the local distance field meandered from the anticipated value. Again the initial solution is used as reference. For this we use the following norm

$$L_{\infty}(\phi) = \max_{\mathbf{x} \in \Omega} |\phi_T - \phi_0|. \quad (48)$$

The convergence data for a sequence of meshes is given in table 1 and is plotted in figure 15. For the triangular mesh the element count used in table 1 and figure 15 is the target line elements along each of the edges of the square. The resulting meshes have 242, 1054, 4262 and 16794 triangular elements and 141, 568, 2212 and 8558 nodes, respectively.

The convergence results are less than expected. For the linear meshes the convergence approaches first order for both norms, while for the quadratic NURBS mesh both norms converge with a slightly higher

Elems	Linear triangle				Linear quad				Quadratic quad			
	$L_1(\hat{H})$	Rate	$L_{\infty}(\phi)$	Rate	$L_1(\hat{H})$	Rate	$L_{\infty}(\phi)$	Rate	$L_1(\hat{H})$	Rate	$L_{\infty}(\phi)$	Rate
10	1.26e-1		3.44e-1		1.34e-1		3.88e-1		1.26e-1		3.06e-1	
20	1.06e-1	0.26	2.54e-1	0.44	1.03e-1	0.38	2.37e-1	0.71	6.19e-2	1.03	1.49e-1	1.04
40	6.80e-2	0.64	1.42e-1	0.84	5.37e-2	0.94	1.20e-1	0.98	1.89e-2	1.72	5.44e-2	1.45
80	3.20e-2	1.09	7.95e-2	0.84	2.52e-2	1.09	6.68e-2	0.85	7.46e-3	1.34	1.78e-2	1.61

Table 1: Convergence of the level-set method.

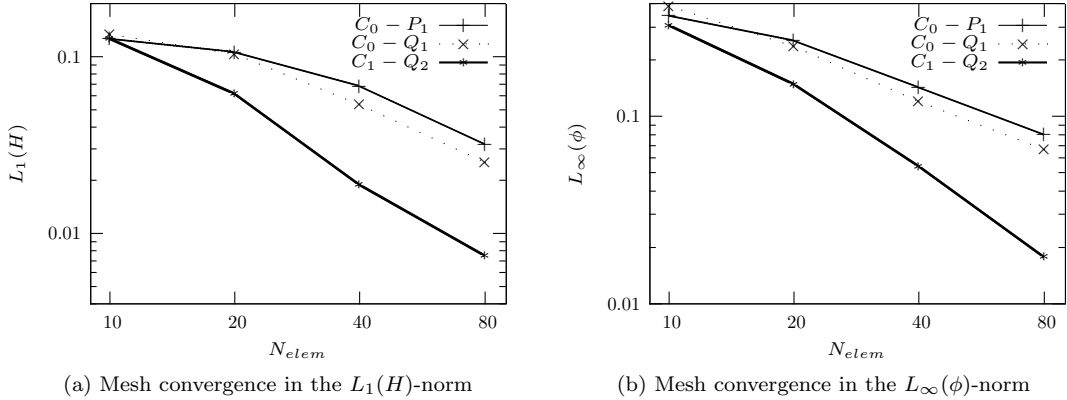


Figure 15: Mesh convergences plots of the *projected inverse scaling* approach.

rate of around 1.5. This is less than is reported in [12]. An explanation could be the difference in volume conservation methodology: local volume conservation is used [12], while here global volume conservation is employed.

6.7. Three-dimensional vortex in a cube

In this section we investigate the applicability of the proposed method in a 3D setting. For this we adopt a 3D version of the vortex in box problem [27]. This results in the following imposed velocity field:

$$\begin{aligned}
 u &= 2 \cos\left(\frac{\pi t}{3}\right) \sin(\pi x)^2 \sin(2\pi y) \sin(2\pi z), \\
 v &= -\cos\left(\frac{\pi t}{3}\right) \sin(2\pi x) \sin(\pi y)^2 \sin(2\pi z), \\
 w &= -\cos\left(\frac{\pi t}{3}\right) \sin(2\pi x) \sin(2\pi y) \sin(\pi z)^2.
 \end{aligned} \tag{49}$$

The level-set experiences a full cycle of deformation in $T = 3.0$, similar as in [29]. The 3D deformation is the superimposed two deformations used in the 2D cases, as given in eq (46). Due to this extreme deformation the volume is spread extremely thin. This is a hard problem to resolve, therefore, we use a mesh with $128 \times 128 \times 128$ linear NURBS elements. Similar to the convergence study we only consider *projected inverse scaling*.

In figure 16 eight snapshots of the $\phi = 0$ level-set are shown. This level-set represents the middle of the interface region. The snapshots at $t = 1.4$ and $t = 1.8$ the volume gets distorted to a high degree, resulting in very thin filaments.

It can be seen in figure 17 the volume is still quite well conserved, although not to full machine precision. To achieve this (near) conservation the required perturbation per timestep is still quite modest, similar as in the 2D case.

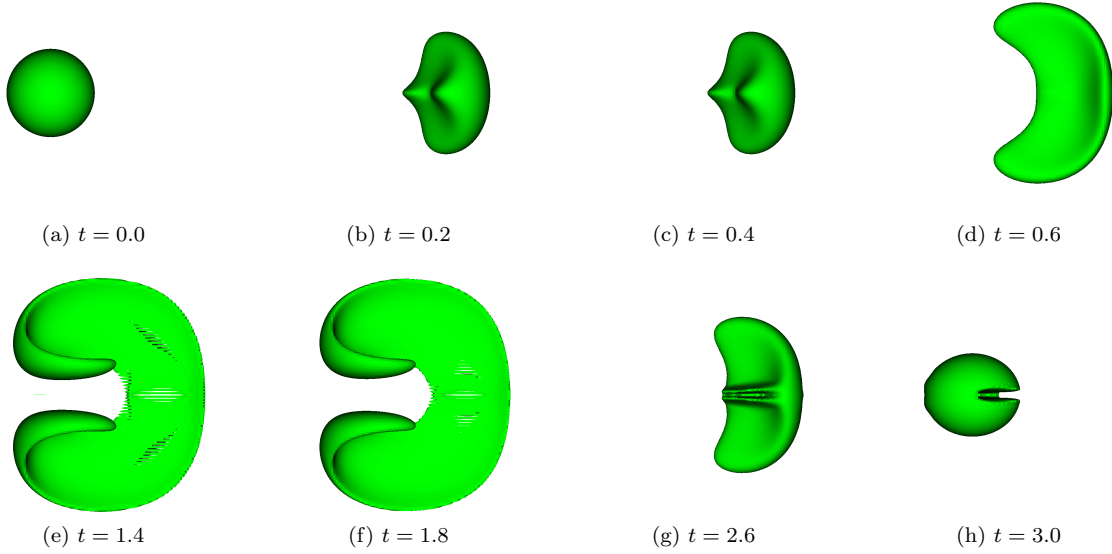


Figure 16: Three-dimensional vortex snapshots on a mesh with 128^3 linear NURBS elements.

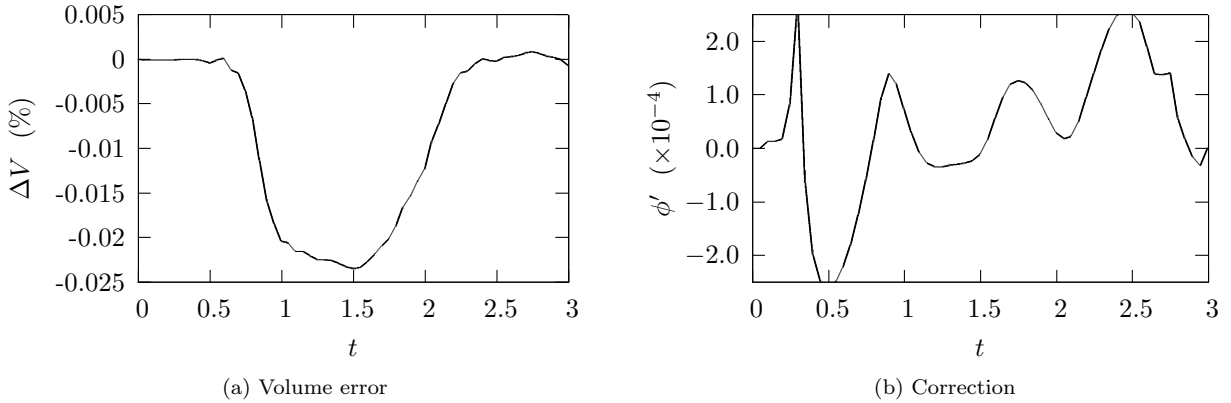


Figure 17: Volume and error and related correction on a mesh with 128^3 linear NURBS elements.

7. Conclusions

In this paper four approaches to obtain a distance field in terms of element lengths have been presented. These approaches attempt to address two issues at the same time. To get truly smooth regularized Heaviside functions on arbitrary meshes, and to get a distance field without solving the difficult Eikonal equations directly.

In order to get smooth Heaviside functions on arbitrary meshes the standard Eikonal equation has been recast in terms of a mesh-metric. Hereby the local meshsize has been taken into account when computing a distance field in terms of element lengths. Solving the Eikonal equation is circumvented by introducing a multiplicative scaling of the level-set. In this paper four different approaches for performing this scaling are investigated. For linear triangular meshes, linear quadrilateral meshes and C_1 -continuous quadratic meshes the following conclusions can be drawn:

- *Direct redistancing.* The original level-set function is corrected using local derivative information. This results in a simple relation for the scaled distance field. However, this approach fails to deliver a smooth Heaviside, even on C_1 meshes. Therefore, despite its simplicity, this approach has to be discarded.
- *Projected redistancing.* The discontinuous scaled distance field from the *direct redistancing* approach is projected on a continuous discretization. This corrects the smoothness issues but introduces other problems. On distorted mesh the use of smoothing results in spuriously diverging contour lines at the boundary. Additionally, in the vortex problem insufficient smoothing results in an irregular solution. However increasing the smoothing leads to excessive problems to conserve the interface location. Therefore, this approach has to be discarded as well.
- *Projected scaling.* Here only the scaling is projected instead of the scaled distance field itself. This solves the problem of excessive interface movement at higher smoothing numbers. Unfortunately, low smoothing can still result in irregular solutions. We conclude that this is in principle a viable approach, but not the most desirable.
- *Projected inverse scaling.* Here the reciprocal value is projected instead of the scaling itself. In this approach the presence of smoothing plays a less prominent roll. In the absence of smoothing the approach still gives high quality solutions. Similar to *projected scaling* the interface is precluded from moving. We conclude that this is approach has all the desired properties and is therefore the preferred choice.

A convergence study has been performed for *Projected inverse scaling*. A L_1 convergence study of the regularized Heaviside function has been done. This is effectively the mismatched area. Additionally, we have considered at the L_∞ norm of the level-set. It has been shown that the method is first order accurate when using linear triangles and quadrilaterals. On quadratic quadrilaterals the method has a slightly higher order of accuracy, approaching an order of 1.5. This slightly reduced order of accuracy might be due to the global volume conservation.

In the future the presented level-set approach will be employed to solve two-fluid flow potentially including (flexible) floating objects. By avoiding a solution of the redistancing problem, the new approaches should facilitate strong coupling of the entire problem. This lays the ground for strict energy control at the two-fluid interface.

Acknowledgements

The author gratefully acknowledges support from Delft University of Technology and Durham University.

References

References

- [1] I. Akkerman, Y. Bazilevs, D.J. Benson, and M.W. Farthing C.E.Kees. Free-surface flow and fluid-object interaction modeling with emphasis on ship hydrodynamics. *Journal of Applied Mechanics*, 2012.
- [2] I. Akkerman, J. Dunaway, J. Kvandal, J. Spinks, and Y. Bazilevs. Toward free-surface modeling of planing vessels: Simulation of the Fridsma hull using ALE-VMS. *Computational Mechanics*, 50(6):719–727, 2012.
- [3] S. Osher and J.A. Sethian. Fronts propagating with curvature-dependent speed: algorithms based on hamilton-jacobi formulations. *Journal of Computational Physics*, 79:12–49, 1988.
- [4] C.A. Felippa, K.C. Park, and C. Farhat. Partitioned analysis of coupled mechanical systems. *Computer Methods in Applied Mechanics and Engineering*, 190(24-25):3247–3270, 2001.
- [5] T.E. Tezduyar. Finite element methods for flow problems with moving boundaries and interfaces. *Archives of Computational Methods in Engineering*, 8(2):83–130, 2001.
- [6] E. Walhorn, A. Kölke, B. Hübner, and D. Dinkler. Fluid-structure coupling within a monolithic model involving free surface flows. *Computers & Structures*, 83(25-26):2100 – 2111, 2005.
- [7] J.A. Sethian and P. Smereka. Level set methods for fluid interfaces. *Annual Review of Fluid Mechanics*, 35(1):341–372, 2003.

- [8] Stanley Osher and Ronald P. Fedkiw. Level set methods: An overview and some recent results. *Journal of Computational Physics*, 169(2):463 – 502, 2001.
- [9] J.A. Sethian. *Level Set Methods and Fast Marching Methods*. Cambridge University Press, 1999.
- [10] S. Osher and R.P. Fedkiw. *Level set methods and dynamic implicit surfaces*. Applied mathematical science. Springer, New York, N.Y., 2003.
- [11] T.J.R. Hughes, J.A. Cottrell, and Y. Bazilevs. Isogeometric analysis: CAD, finite elements, NURBS, exact geometry, and mesh refinement. *Computer Methods in Applied Mechanics and Engineering*, 194:4135–4195, 2005.
- [12] I. Akkerman, Y. Bazilevs, C. Kees, and M. Farthing. Isogeometric analysis of free-surface flow. *Journal of Computational Physics*, 2011. Published online. doi:10.1016/j.jcp.2010.11.044.
- [13] C. Kees, I. Akkerman, M. Farthing, and Y. Bazilevs. A conservative level set method suitable for variable-order approximations and unstructured meshes. *Journal of Computational Physics*, 2011. Published online. doi:10.1016/j.jcp.2011.02.030.
- [14] E. Marchandise and J.-F. Remacle. A stabilized finite element method using a discontinuous level set approach for solving two phase incompressible flows. *Journal of Computational Physics*, 219(2):780 – 800, 2006.
- [15] J.A. Sethian. Evolution, implementation, and application of level set and fast marching methods for advancing fronts. *Journal of Computational Physics*, 169:503–555, 2001.
- [16] A.N. Brooks and T.J.R. Hughes. Streamline upwind/Petrov-Galerkin formulations for convection dominated flows with particular emphasis on the incompressible Navier-Stokes equations. *Computer Methods in Applied Mechanics and Engineering*, 32:199–259, 1982.
- [17] J.-L. Guermond and M. Nazarov. A maximum-principle preserving finite element method for scalar conservation equations. *Computer Methods in Applied Mechanics and Engineering*, 272:198 – 213, 2014.
- [18] V. John and P. Knobloch. On spurious oscillations at layers diminishing (sold) methods for convection-diffusion equations: Part I - a review. *Computer Methods in Applied Mechanics and Engineering*, 196(17-20):2197 – 2215, 2007.
- [19] J.-L. Guermond, R. Pasquetti, and B. Popov. Entropy viscosity method for nonlinear conservation laws. *Journal of Computational Physics*, 230(11):4248 – 4267, 2011. Special issue High Order Methods for {CFD} Problems.
- [20] S. Balay, S. Abhyankar, M.F. Adams, J. Brown, P. Brune, K. Buschelman, V. Eijkhout, W.D. Gropp, Dinesh Kaushik, M. G. Knepley, L.C. McInnes, K. Rupp, B.F. Smith, and H. Zhang. PETSc Web page. <http://www.mcs.anl.gov/petsc>.
- [21] S. Balay, S. Abhyankar, M.F. Adams, J. Brown, P. Brune, K. Buschelman, L. Dalcin, V. Eijkhout, W.D. Gropp, D. Kaushik, M.G. Knepley, L. Curfman McInnes, K. Rupp, B. F. Smith, S. Zampini, and H. Zhang. PETSc users manual. Technical Report ANL-95/11 - Revision 3.6, Argonne National Laboratory, 2015.
- [22] J.A. Cottrell, T.J.R. Hughes, and Y. Bazilevs. *Isogeometric Analysis: Toward Integration of CAD and FEA*. Wiley, Chichester, 2009.
- [23] L. Piegl and W. Tiller. *The NURBS Book (Monographs in Visual Communication)*, 2nd ed. Springer-Verlag, New York, 1997.
- [24] Y. Bazilevs, L. Beirao da Veiga, J.A. Cottrell, T.J.R. Hughes, and G. Sangalli. Isogeometric analysis: Approximation, stability and error estimates for h -refined meshes. *Mathematical Models and Methods in Applied Sciences*, 16:1031–1090, 2006.
- [25] J.A. Evans, Y. Bazilevs, I. Babuška, and T.J.R. Hughes. N-widths, sup-infs, and optimality ratios for the k-version of the isogeometric finite element method. *Computer Methods in Applied Mechanics and Engineering*, 198:1726–1741, 2009.
- [26] Ch. Geuzaine and J.-F. Remacle. Gmsh: A 3-d finite element mesh generator with built-in pre- and post-processing facilities. *International Journal for Numerical Methods in Engineering*, 79(11):1309–1331, 2009.
- [27] R.J. LeVeque. High-resolution conservative algorithms for advection in incompressible flow. *SIAM Journal on Numerical Analysis*, 33(2):627–665, 1996.
- [28] W.J. Rider and D.B. Kothe. Reconstructing volume tracking. *Journal of Computational Physics*, 141:112–152, 1998.
- [29] R.N. Elias and A.L.G.A. Coutinho. Stabilized edge-based finite element simulation of free-surface flows. *International Journal for Numerical Methods in Fluids*, 54(6-8):965–993, 2007.